



Thermal decomposition of JP-10 studied by micro-flowtube pyrolysis-mass spectrometry

Shamit Nakra, Richard J. Green¹, Scott L. Anderson*

Department of Chemistry, University of Utah, 315 S. 1400 E. Rm 2020, Salt Lake City, UT 84112, USA

Received 1 February 2005; received in revised form 10 July 2005; accepted 11 August 2005

Available online 17 November 2005

Abstract

Decomposition of JP-10 (exo-tetrahydrodicyclopentadiene) was studied in a small flowtube reactor over the temperature range up to ~ 1700 K on the millisecond time scale. For comparison, the decomposition behavior of cyclopentadiene, dicyclopentadiene, and benzene was studied under identical conditions. Products of pyrolysis were identified by chemical ionization (CI) and electron impact ionization (EI) mass spectrometry. On the experimental time scale, JP-10 begins to decompose above 900 K and is completely decomposed by 1300 K. In the initial decomposition, the principal products are cyclopentadiene, benzene, propyne, and C_4H_x . At high temperatures, the cyclopentadiene decomposes, and the principal species observed are benzene, acetylene, and ethylene. From the combination of EI and CI spectra, we can confirm that the C_6 product observed is benzene, with few if any other C_6H_x products. Similarly, the C_5 product is cyclopentadiene, with no cyclopentene or other C_5H_x products. The observed product distribution is inconsistent with both equilibrium speciation and predictions of existing JP-10 kinetic models.

© 2005 The Combustion Institute. Published by Elsevier Inc. All rights reserved.

Keywords: JP-10; Pyrolysis; Kinetics; Mass spectrometry; Breakdown; Combustion

1. Introduction

JP-10 is a synthetic high-energy-density fuel used in missile applications and in many combustion research studies [1–15]. It is chiefly composed of a single compound, exo-tetrahydrodicyclopentadiene (exo-THDCP; IUPAC name: tricyclo[5.2.1.0^{2,6}]decane), and therefore is simpler to study than typical

refined hydrocarbon fuels, which are complex mixtures that may vary from source to source. Good data are available on thermochemical, rheological, and other physical properties [2,4,16–23]. On the other hand, relatively little is known regarding the detailed combustion mechanism. Rate constants have been reported for reaction of JP-10 with OH, O₂, and O₃ [4,17,20], but only at room temperature. Shock-tube measurements have been performed on JP-10 ignition, which provide information on the kinetics of the combustion but not detailed information about the chemical species involved [24,25]. Williams and co-workers [1] have suggested a mechanism in which the first step of THDCP breakdown proceeds by breaking a C–C bond common to two five-membered rings,

* Corresponding author.

E-mail address: anderson@chem.utah.edu (S.L. Anderson).

¹ Current address: Battelle Dugway Operations, West Desert Test Center, P.O. Box 217, Dugway Proving Ground, UT 84022, USA.

and eventual breakdown to acetylene and ethylene. Davidson et al. [25] conclude from shock-tube measurements and kinetic modeling that C_2 species probably play an important role in the decomposition of JP-10. Information regarding product speciation as a function of temperature is important both in guiding development of combustion models, and in development and interpretation of optical diagnostics for JP-10 ignition/combustion. Our experiments are aimed at providing this information.

2. Experimental approach

The micro-flowtube reactor/mass spectrometer instrument (micro-FTRMS) has been described in detail in previous publications on pyrolysis of quadricyclane and cubanes [26,27]. For these experiments, JP-10 was diluted in either argon or helium buffer gas at ~3% molar concentration by bubbling the rare gas through liquid JP-10 at room temperature. The mixture was then metered into a small flowtube reactor at a total pressure of a few hundred pascal (see below).

To work at the higher temperatures needed to decompose JP-10, our original quartz flowtube was replaced with an alumina tube (2.39 mm ID) heated by external tantalum windings potted in ceramic cement, capable of prolonged operation at 1800 K. The alumina tube is ~30 cm long, but only the final ~10 cm is heated, allowing transition to laminar flow prior to entering the hot zone. During reaction runs, the temperature is measured continuously by a thermocouple cemented against the outside wall of the alumina tube. To calibrate this external thermocouple with respect to the internal wall temperature, separate calibration runs were carried out, in which a second thermocouple was inserted inside the flowtube bore. This calibration is checked periodically to verify that the external thermocouple reading is not affected by aging of the heater and ceramic potting material. No gas is flowed during the calibration runs; however, the gas has negligible cooling effects at the low pressures and flow rates used in our experiments. Similarly, the concentration of JP-10 in the buffer gas is far too low for the pyrolysis endothermicity to cause significant cooling. The inside thermocouple is removed during reaction runs to avoid reactions on the metal thermocouple surfaces. To verify that the temperature is uniform over the hot zone of the tube, a flowtube with several external thermocouples was tested. We conclude that the temperature is constant and accurate to ~5 K over the central 90% of the hot zone length.

The flowtube exhaust is dumped into a sealed, temperature-stabilized (~200 °C) ionization source where analyte molecules can be ionized either by electron impact ionization (EI) or by methane chemi-

cal ionization (CI). The total source pressure is either 47 or 200 Pa for EI and CI, respectively. The flowtube is inserted into a 3-mm-deep counterbore in the ion source, so that it does not make direct contact. There is a 0.05-mm annular gap between the flowtube and counterbore, creating a connection with low thermal conductivity but also with low conductance for gas loss. The main points whereby gas can exit the source are a 0.99-mm orifice where ions exit the source and a 0.55-mm orifice where a magnetically collimated electron beam is injected into the source to cause ionization. For EI, the electron beam ionizes the analyte molecules directly, using electrons with nominal kinetic energy of 75 eV, which was found to give the best intensity for near-molecular-weight ions. This energy is also close enough to the 70 eV energy used in the standard mass spectra compiled in the NIST database [28] so that the standard spectra can be used in analysis of the pyrolysis products.

For CI, methane is injected into the ion source through a separate inlet; i.e., there is no methane entering the flowtube reactor. In the source, the methane:argon:JP-10 pressure ratio is approximately 87:12:1. Electrons are injected into the source, where they predominantly ionize the methane. Ion–molecule reactions in the methane generate a series of low-mass hydrocarbon reagent ions, the most abundant being CH_5^+ . In collisions with most molecules (M), the proton transfer reaction: $M + CH_5^+ \rightarrow (M + H)^+ + CH_4$ is exoergic, and proceeds on every collision (see below). The advantage of CI is that it is a relatively gentle ionization method. For many molecules, CI results in a spectrum consisting primarily of the $(M + H)^+$ ion, making identification of the parent mass (M) trivial. A major disadvantage of CI is that the low mass region of the CI spectrum is dominated by the hydrocarbon reagent ions, interfering with detection of low mass species. In addition, CI spectra, while quite reproducible in any given instrument, vary significantly with ion source design and operating conditions. For this reason no database of “standard” CI spectra is available to aid spectral assignments. Analysis of EI spectra is complicated by extensive fragmentation; however, standard spectral libraries are available to guide identification [28]. After exiting the ion source, the ions are analyzed by a tandem mass spectrometer, operated for these experiments as a single-stage mass spectrometer.

For CI, argon is bubbled through JP-10 at room temperature, generating a reactant flow that is ~2.6% JP-10. For EI, helium is used with pressure resulting in a JP-10 concentration of 3.9%. The reactant mix is metered through a glass/Teflon leak valve into the flowtube, where the pressure drops to a few hundred pascal. Because this valve is not adjusted during a set of experiments, the total mass flow rate through the

Table 1
Flowtube properties under chemical ionization (CI) and electron impact ionization (EI) conditions

T (K)	P_{midpoint} (Pa)	Density (mol/m ³)	Velocity (m/s)	Residence time (ms)
CI conditions				
298	274	0.11	10.7	9.35
898	336	0.05	26.3	3.81
1498	389	0.03	37.9	2.64
EI conditions				
298	181	0.07	16.2	6.18
898	254	0.03	34.9	2.87
1498	309	0.02	47.7	2.10

reactor is independent of temperature, as verified by constant source chamber gas load. On the other hand, the hot zone gas density and flow velocity do change with flowtube temperature. The density, pressure, and flow velocity at the flowtube midpoint, together with the calculated hot zone residence time, are shown in Table 1. Flow properties were calculated assuming incompressible flow, which is reasonable in light of the low flow velocities. As the table shows, to avoid entry of methane into the flowtube, it is necessary to increase the pressure in the flowtube by ~50%, also affecting other flow properties.

From the density and gas (mostly Ar or He) viscosity, the diffusion constant can be calculated and used to estimate the average distance the JP-10 molecules will diffuse during the residence time in the hot zone. This turns out to be 50 to 70 mm for EI conditions, and 20 to 30 mm for CI conditions. This diffusion length is substantially larger than the flowtube diameter; thus the JP-10 molecules clearly diffuse across the tube bore many times during passage through the hot zone. There are several consequences. The flow can be treated as pseudo-plug flow; i.e., all sample molecules have equal residence times in the hot zones. In addition, collisions with the flowtube wall mean that the JP-10 molecular temperature should track the wall temperature quite closely.

Wall collisions also lead to the possibility of wall-catalyzed reactions. We have examined chemistry in both alumina and silica tubes, and also in a tube with larger diameter, higher pressure, and higher flow velocities, where the number of wall collisions reduced substantially (but not to zero). The product distributions are essentially identical in all cases, at least up to the maximum working temperature of the silica tube (~1300 K). The tube walls are observed to develop a light gray color during the initial pyrolysis run, presumably because of carbon deposition on the walls. Once this carbon layer forms, it does not thicken noticeably in months of operation. The only suggestion of unique wall chemistry in the JP-10 system is that various primary products are observed to undergo dehydrogenation at temperatures above 1500 K, and this

chemistry probably is wall-catalyzed. We conclude that there is substantial initial wall chemistry for clean silica or alumina surfaces, but that carbon deposition passivates the surface, and wall chemistry thereafter is important only at temperatures well above the breakdown temperature of JP-10.

Two samples of JP-10, both obtained from Koch Petroleum, were examined. Prior to analysis in the flowtube reactor, both samples were analyzed for purity via gas chromatography–mass spectrometry (GC–MS). One sample was commercial, Mil-Spec JP-10, which includes stabilizers. This sample elutes from the GC in four components with elution times from 4.5 to 5 min. The main peak (~76% of the total intensity) at 4.72 min is identified as the exo-THDCP isomer and gives a mass spectrum similar to those shown below. Another peak (~8%), eluting at just over 5 min, has a nearly identical mass spectrum and is therefore identified as the endo-THDCP isomer. The other two GC peaks (each ~8%) give mass spectra with major peaks near the molecular weight of exo-THDCP (136 amu); however, there is considerably less fragmentation, suggesting that these contaminants are less strained isomers. Because the purity of this commercial JP-10 sample was only ~76%, all the flowtube reaction data below were taken using a sample of freshly synthesized, unstabilized JP-10 that was distilled by Koch Petroleum to higher purity than the commercial-grade product. GC–MS analysis shows this sample to be about 96% pure exo-THDCP.

A few authors have studied the mass spectra of exo-THDCP [18,19]. Inman and Serve [18] studied the fragmentation of exo-THDCP with electron impact ionization (EI) at 70 eV after gas chromatographic separation. They found large fragment peaks at masses 121, 95, 94, 79, and 67. Herzschuh et al. [19] also studied the EI fragmentation pattern at electron energies of both 70 and 14 eV. At 70 eV, the parent peak is only at 8.4%, but grows to 36.9% at 14 eV. At 14 eV, they find large fragment peaks at 121, 108, 95, 94, and 66 amu. Our EI mass spectrometry results below are generally consistent with the previous data. The small differences in relative intensities

of fragment ions probably reflect differences in source temperature and the presence of He buffer gas in our EI experiments.

3. Results and discussion

3.1. The CI fingerprint of JP-10

Pyrolysis studies were conducted on the high-purity JP-10 sample, and also on related compounds considered to be possible products of JP-10 pyrolysis. Comparison of the temperature-dependent mass spectra of these compounds with the JP-10 pyrolysis mass spectra allows us to assign the identity of the products with reasonable confidence. The EI data discussed in the next section provide corroborating evidence, and allow examination of the low mass region of the product distribution. Fig. 1 shows a series of methane chemical ionization (CI) mass spectra after JP-10 in argon was passed through the flowtube at different temperatures (right-hand scale). The spectra were actually scanned over the mass range up to 300 amu to check for adducts or species that might result from polymerization on the flowtube walls. No significant peaks were observed above 140 amu.

The bottom spectrum is for the flowtube at room temperature (right-hand scale), where no decomposition occurs. This spectrum shows the CI fingerprint of JP-10 itself; i.e., all the mass peaks observed result from CI of intact JP-10 entering the ion source. In addition to a weak molecular mass peak (136 amu), the CI mass spectrum is dominated by a characteristic set of fragment ion peaks. The important CI fragment masses and the corresponding net atom losses

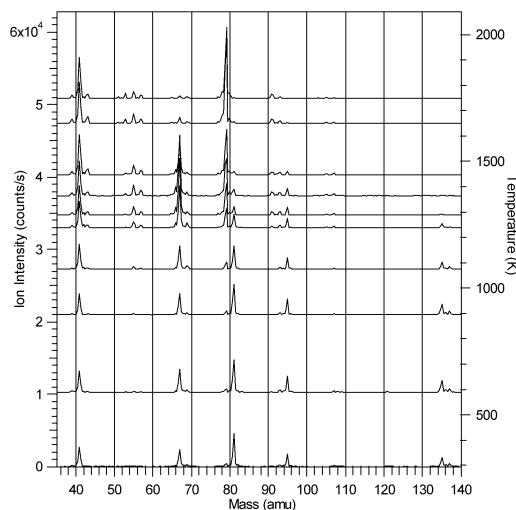


Fig. 1. Pyrolysis mass spectra of JP-10 by chemical ionization.

from $(M + H)^+$ are 135 ($-H_2$), 95 ($-C_3H_6$), 81 ($-C_4H_8$), and 67 ($-C_5H_{10}$). There is also a prominent peak at 41 ($C_3H_5^+$), corresponding to loss of C_7H_{12} from $(M + H)^+$. Mass 41 is also prominent in the background spectrum of hydrocarbon CI reagent ions; however, the changes in mass 41 intensity with temperature indicate real signal at this mass. This conclusion is verified by the EI spectra (below).

It is somewhat unusual for a molecule to fragment so extensively in CI. Mass spectral data provide no information on fragmentation pathways; e.g., loss of C_5H_{10} could come from any combination of neutral species adding up to the correct mass. Nonetheless, it is possible to rationalize the observed pattern theoretically. To help understand the JP-10 fragmentation, we carried out the following ab initio calculations, using GAUSSIAN 98 [29]. The JP-10 (i.e., *exo*-THDCP) structure was first optimized at the B3LYP/6-31G* level of theory; then the effect of protonation (the dominant ionization pathway in methane CI) was examined in two steps. In the first step, a proton was added to one of the six distinguishable carbon atom sites in JP-10 (labeled 1 through 6 in Fig. 2); then the geometry was reoptimized with the carbon skeleton frozen. The energy difference between the resulting structures and the JP-10 structure gives a rough estimate of the vertical proton affinity (i.e., the proton affinity in the absence of isomerization/skeletal relaxation). The values are quite similar for all carbon sites, ranging from 6.87 eV for site 6 to 6.54 eV for site 5. From the point of view of detection efficiency, the important point is that the adiabatic proton affinities at all carbon sites are significantly larger than those of CH_4 (5.49 eV [30]) so that the proton transfer ionization process should be efficient. Because the energies are so similar, it is not unreasonable to assume that

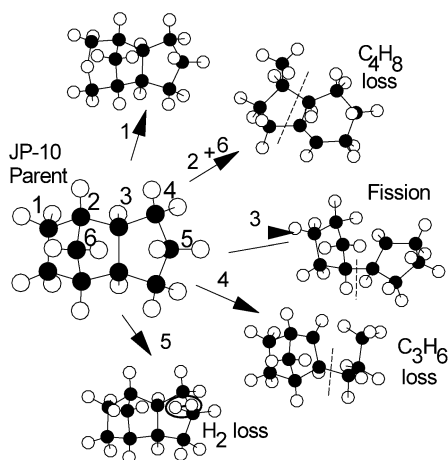


Fig. 2. Ab initio proton-induced decomposition pathways for JP-10.

protonation occurs at every site, depending mainly on collision orientation.

Each geometry was then reoptimized with all atoms free to move. The resulting structures provide insight into the protonation-induced fragmentation processes and provide adiabatic proton affinities, which range from 6.6 eV for protonation at site 5 to 8.7 eV for sites 2 or 6. Protonation is calculated to result in dramatic changes in JP-10 structure (Fig. 2), and the resulting structures allow us to rationalize the main features of the observed fragmentation pattern. Protonation at site 1 leads to a C–H–C bridge-bonded structure. Protonation at sites 2 or 6 leads to rearrangement of the carbon skeleton, generating a structure with fused 5- and 6-membered rings. This structure might lose C_4H_8 as indicated, providing a plausible route to the observed mass 81 ion. Protonation at site 3 leads to a structure with two C_5 rings connected by a single bond. Cleavage of this bond, accompanied by hydrogen migration or loss, could generate the mass 67 ion. Protonation at site 4 results in a structure that, with H migration, could lose C_3H_6 , generating the mass 95 ion, and protonation at site 5 sets the system up to lose H_2 (circled in Fig. 2), which would generate the mass 135 ion. Some of these pathways require H-migration prior to or during fragmentation; however, such migration is typically easy in hydrocarbon cations. The peak observed for the $(M + H)^+$ parent ion may result from protonation at site 1, where there is no obvious carbon fragment loss mechanism, or may represent a small fraction of unfragmented ions remaining from protonation at other sites.

3.2. Variable temperature CI—JP-10 pyrolysis

In Fig. 1, the mass spectra are temperature-independent for $T < 1000$ K, but at higher temperatures, changes in the mass spectra indicate that JP-10 is breaking down. In particular, certain peaks characteristic of JP-10 (e.g., mass 81, the group of peaks at 135–137) decrease in intensity, disappearing completely above ~ 1300 K. The disappearance of these peaks indicates that JP-10 decomposes on the millisecond time scale in this temperature range. At the same time, new peaks grow in, indicating the presence of pyrolysis products. There are a group around mass 55, corresponding to C_4 species, a large peak at mass 79, corresponding to $C_6H_7^+$, and peaks at 91 and 93, corresponding to C_7 products. There are also groups of peaks corresponding to C_8 , C_9 , and C_{10} products; however, these contribute a negligible fraction of the total product signal. Some mass peaks clearly appear in the spectra of both JP-10 and its pyrolysis products. For example, mass 67, corresponding to $C_5H_7^+$, is a major peak in the JP-10 spectra at low temperatures,

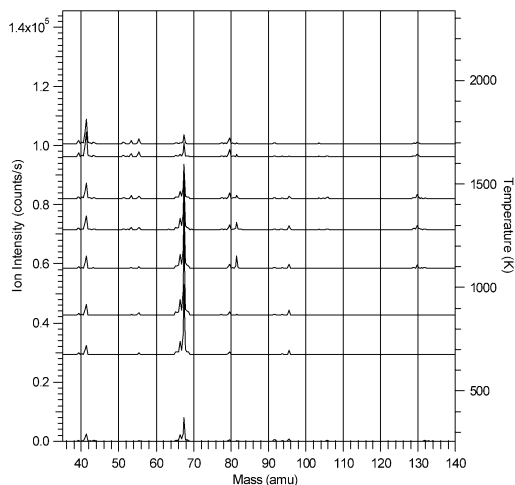


Fig. 3. Pyrolysis mass spectra of cyclopentadiene (CPD) by chemical ionization.

but also appears (with increased intensity) at temperatures above 1300 K, where JP-10 is completely decomposed. The implication is that $C_5H_7^+$ is produced both in CI-induced fragmentation of JP-10 and in CI of some pyrolysis product(s).

From fitting the temperature dependence of the disappearance of the JP-10 fingerprint peaks, it is straightforward to determine the breakdown vs temperature behavior of JP-10. In addition, however, we want to determine the product distribution as a function of temperature. For this purpose, we also studied pyrolysis mass spectra of various species that might be expected to be products, as well as species suggested by the major peaks in the high-temperature JP-10 results. One major product peak is that at mass 67. This $C_5H_7^+$ ion might result from proton transfer ionization of a C_5H_6 pyrolysis product, or from protonation-induced fragmentation of a higher-mass pyrolysis product. By far, the most stable C_5H_6 compound is cyclopentadiene (CPD), and it is not difficult to imagine pathways by which this product might be generated from JP-10. Fig. 3 gives the CI pyrolysis mass spectra of CPD, taken under conditions identical to those used for JP-10. It turns out that in the bulk, CPD is in equilibrium with its dimer, thus the CPD vapor passing into the flow-tube contains a small fraction of CPD dimer; giving rise to a set of barely visible peaks at masses just above 130. The main peak in the low-temperature CI spectrum of CPD is mass 67 ($CPD + H^+$), with a smaller peak at 66 (CPD^+), and several small peaks corresponding to adducts or fragments of adducts. The CPD^+ peak probably results from direct electron impact ionization in our relatively low-pressure CI source. The adduct peaks result from reactions with some of the hydrocarbon reagent cations gener-

ated in the CI process. For example, the peaks at 95 and 79 are attributed to $(\text{CPD} + \text{C}_2\text{H}_5^+)$ and $(\text{CPD} + \text{C}_2\text{H}_5^+ - \text{CH}_4)$, respectively, and 41 is attributed to $(\text{CPD} + \text{CH}_5^+ - \text{C}_3\text{H}_6)$.

Note that in the pyrolysis mass spectra of CPD (Fig. 3), the mass 67 peak diminishes at high temperatures, with concomitant growth in the mass 41 peak, indicating that CPD pyrolyzes above ~ 1500 K on the experimental time scale, apparently losing C_2H_2 to generate C_3H_4 . C_3H_4 is then ionized by proton transfer, yielding a mass 41 ion. Similar trends are observed for the mass 67 and 41 peaks in the pyrolysis mass spectra of JP-10 (Fig. 1), suggesting that CPD is the dominant carrier of the mass 67 signal, i.e., that CPD is a major JP-10 pyrolysis product. The EI mass spectra below provide further support for identifying CPD as a major JP-10 pyrolysis product.

One of the largest peaks in the JP-10 CI spectra at high T is at mass 79. This peak suggests a pyrolysis product with empirical formula C_6H_6 (C_6H_7^+ when protonated), and the only compounds with high enough stability to be likely products are benzene (BEN, $\Delta H_f = 82.9$ kJ/mol) and methylene cyclopentadiene (MCPD, $\Delta H_f = 223.8$ kJ/mol). Whatever this product is, it must be quite thermally stable, because the mass 79 peak remains substantial at the highest temperatures. For comparison, Fig. 4 gives the variable-temperature CI mass spectra for benzene (BEN). Note the intense peak at mass 79, corresponding to protonated benzene, and note that mass spectrum is nearly temperature-independent, showing signs of decomposition only at ~ 1800 K. Such a mass spectrum is consistent with the persistence of the mass 79 peak in the high-temperature JP-10 spectra,

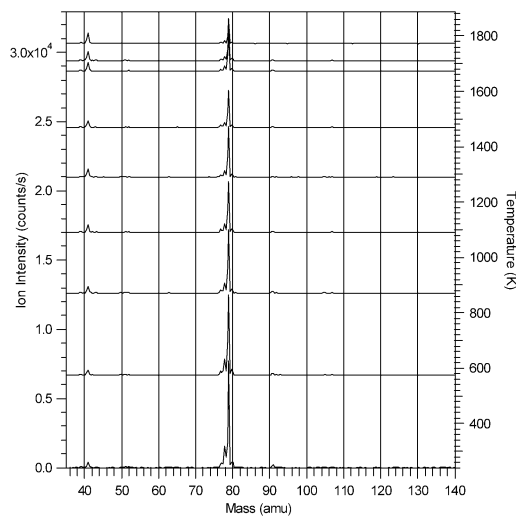


Fig. 4. Pyrolysis mass spectra of benzene by chemical ionization.

suggesting that benzene is a major high-temperature pyrolysis product. We were unable to run spectra of MCPD for comparison, as this compound is not commercially available; however, its considerably higher ΔH_f makes it quite unlikely that MCPD could be a JP-10 product, particularly at the higher temperatures. The CI peak at 79 could conceivably come from CI-induced fragmentation of some pyrolysis product of higher molecular weight; however, the EI data (below) rule out significant JP-10 breakdown into such products. The conclusion is that benzene is a major pyrolysis product, which is somewhat surprising because generation of benzene requires significant skeletal rearrangement. The lowest-energy pathways to benzene from JP-10 probably correspond to production of C_4 species, and mass peaks corresponding to C_4H_x appear over the same temperature range where benzene is first observed. At temperatures near 1200 K, the dominant C_4 peaks correspond to C_4H_7^+ (55) and C_4H_9^+ (57). If we assumed that these represented protonated molecular ions, this would imply that the product distribution contained one or more species with empirical formulae C_4H_6 and C_4H_8 (plus C_4H_4 at the highest temperatures). It is entirely possible, however, that the CI spectrum of the C_4H_x product(s) is complicated by H_2 elimination from the nascent protonated molecular ion.

JP-10 is produced by hydrogenating the CPD dimer ($\text{C}_{10}\text{H}_{12}$), raising the question of whether CPD dimer might serve as an intermediate in the pyrolysis process. Although too small to see in Fig. 1, there is a group of peaks appearing at mass 129 and 131 at the highest temperatures, suggesting a minor dehydrogenation product channel (probably wall-catalyzed) that turns on at high temperatures. Fig. 5 shows a

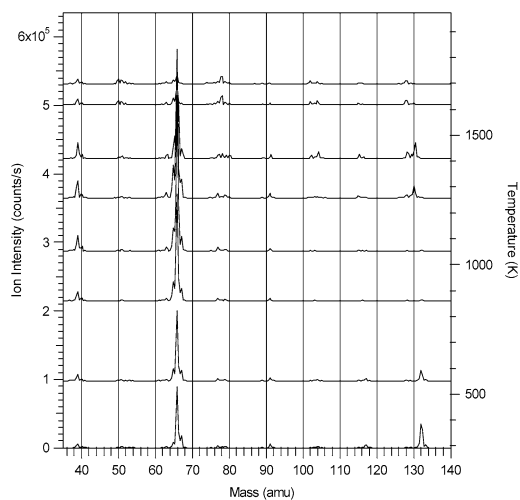
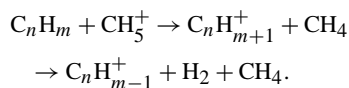


Fig. 5. Pyrolysis mass spectra of CPD dimer by electron impact.

set of pyrolysis mass spectra of CPD dimer for comparison. EI was used in this case because we found that CPD dimer tends to hydrogenate under CI conditions. As already noted, CPD and the CPD dimer are in equilibrium at room temperature. For this experiment, CPD dimer crystals were collected from the bottom of a container of CPD liquid, placed in a sample container on the flowtube inlet system and then heated and pumped on to remove the more volatile monomer. The dimer \rightleftharpoons monomer reequilibration is slow; thus it is possible to enrich the vapor phase significantly with CPD dimer, provided that the pumping operation is repeated periodically. The vapor entering the flowtube still contains a substantial monomer concentration, but the thermal and mass spectral behavior of the dimer can be inferred by comparison with the monomer data (Fig. 3). In particular, there is a peak at mass 132, the CPD dimer molecular mass. Note that the 132 peak disappears completely by 800 K, indicating easy decomposition of the dimer, mostly by fission to CPD monomer. The temperature 800 K is well below that at which JP-10 begins to decompose; therefore, CPD dimer can be ruled out as a JP-10 pyrolysis product. Note, however, that at high temperatures, dehydrogenation products are observed for CPD dimer at 128 and 130, probably from decomposition on the flowtube walls. Under CI conditions, these peaks would appear at 129 and 131, matching the minor peaks observed in the high-temperature JP-10 spectra. The conclusion is that while CPD dimer itself is not present in the JP-10 pyrolysis products, dehydrogenation, possibly involving CPD dimer as an intermediate, is a minor JP-10 pyrolysis pathway at high temperatures, generating products such as $C_{10}H_{10}$ and $C_{10}H_8$.

3.3. Electron impact studies of JP-10 pyrolysis

There are several drawbacks to the use of methane CI in JP-10 pyrolysis studies. One, already noted, is that masses below ~ 40 are inaccessible because of high background. In addition, the lack of standard CI spectra for comparison can raise questions regarding spectral assignments. For example, the two main product ions, $C_5H_7^+$ and $C_6H_7^+$, are highly stable ions, raising the possibility that they might originate from fragmentation of a higher-mass neutral. In particular, it is not uncommon to lose H_2 in proton transfer CI:



It is conceivable, therefore, that some or all of the $C_5H_7^+$ CI signal might originate from C_5H_8 rather

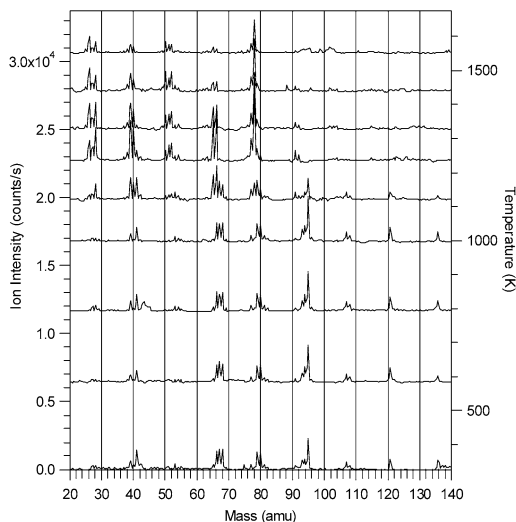


Fig. 6. Pyrolysis mass spectra of JP-10 by electron impact (EI).

than CPD, or that the $C_6H_7^+$ CI signal might have contributions from products heavier than benzene. The fact that the temperature dependence of the CPD and benzene CI spectra is consistent with the JP-10 results supports, but cannot prove, the assignments.

To address these problems, we also studied JP-10 pyrolysis, detecting products with electron impact ionization (EI). For typical hydrocarbons, EI results in extensive production of fragment ions, dependent on both the molecule and the electron energy. While the fragmentation accompanying EI can complicate spectral assignments, the great advantage is that the fragmentation patterns are not strongly dependent on the instrument, and libraries of EI mass spectra for thousands of compounds are available for comparison with unknown spectra [28].

The JP-10 pyrolysis EI spectra are shown in Fig. 6. Consider the room-temperature spectrum, i.e., the fingerprint spectrum for pure JP-10. The extensive fragmentation observed is consistent with the photoionization experiments of Fedorova et al. [16,31] who found that a variety of C_5 , C_6 , C_7 , C_8 , and C_9 fragment ions have appearance energies within 1 eV of the JP-10 ionization energy.

The EI spectra confirm the conclusions derived from the CI data. Most importantly, the JP-10 breakdown temperature dependence inferred from the EI and CI spectra is nearly identical. The EI data also corroborate the assignments of CPD and benzene as the only significant C_5 and C_6 pyrolysis products. In particular, the EI data definitively rule out any significant contributions to the pyrolysis product distribution from C_5H_x or C_6H_x ($x > 6$) isomers. Consider C_5H_8 . All 17 of the C_5H_8 isomers listed in the NIST mass spectral database [28] give strong peaks at

mass 67 and 68 under standard 70 eV EI conditions. In the EI spectra of JP-10 at high flowtube temperatures, where JP-10 is completely decomposed, the only peaks in the C_5 mass range are at 65 and 66, eliminating the possibility that any of the C_5H_8 isomers is present in significant concentration. Based on the analogous data for C_5H_{10} and for C_6H_x , $x = 8, 10$, we can conclude that the only significant C_5 and C_6 products are CPD and benzene, respectively.

This issue is important in light of the tentative conclusion from Hanson and co-workers [32] that cyclopentene, rather than CPD, is produced in their JP-10 shock tube experiments. While it is possible that the difference reflects the higher temperatures and pressures in the shock experiments, we also note that their assignment was based on UV absorption spectroscopy. Assigning the broad UV spectrum observed for a mixture of hydrocarbons at high temperatures is a challenging problem. Unambiguous spectral assignment would require detailed simulations of the vibrational hot band structure for all the hydrocarbons that might be present. Because the high (and anharmonic) vibrational levels populated at high temperatures are poorly characterized, such detailed analysis is not generally feasible.

The EI spectra also allow us to probe low-molecular-weight pyrolysis products, although the analysis is complicated by EI-induced fragmentation of high-molecular-weight species into low-mass ions. Note that even at room temperature, where JP-10 is the only hydrocarbon entering the ion source, there is substantial ion signal in the mass range below 50, mostly in the range around 40. It is clear that as the temperature is raised and JP-10 breaks down, the intensity of low-mass ions increases substantially, implying that the increases result from EI of some pyrolysis product. Consider, for example, the temperature dependence of the mass 26 signal. This mass has negligible intensity at low temperatures, but is one of the major peaks in the high-temperature EI spectrum. Before concluding that acetylene is a major pyrolysis product, however, we need to account for contributions to the high-temperature mass 26 signal from EI-induced fragmentation of heavier pyrolysis products, such as CPD, benzene, C_4H_x , or C_3H_4 —all identified in the high-temperature CI spectra. Here, we take advantage of the existence of the extensive NIST library of EI mass spectra [28]. Note that in the high-temperature JP-10 EI spectra, mass 26 is considerably more intense than 27. For CPD, benzene, and all common isomers of C_4H_x and C_3H_4 , the EI fragmentation patterns have considerably higher intensity for 27 than 26. The implication is that EI-induced fragmentation of the pyrolysis products contributes only a small fraction of the mass 26 intensity. The same is true for EI-induced fragmentation of C_2H_4 ,

which is shown below to be a major pyrolysis product, not detectable by CI. We can conclude, therefore, that acetylene is an important high-temperature JP-10 pyrolysis product. By “important product” we do not mean that acetylene necessarily forms directly by JP-10 fragmentation, but only that it is produced in the flowtube chemistry, rather than simply by fragmentation in the mass spectrometer ionizer. The acetylene peak begins to appear at ~ 1100 K, just above the temperature where JP-10 begins to decompose, suggesting that there may be some direct production from JP-10. The observation in CI that the CPD product undergoes secondary decomposition generating C_3H_4 , suggests that acetylene is probably also generated in the CPD breakdown at high temperatures.

The other major low-mass peak at high temperatures is mass 28, $C_2H_4^+$. In this case, the important point to note is that 28 appears in the high temperature JP-10 spectra with much higher intensity than the neighboring mass 27 and 29 peaks. Standard EI mass spectra of likely C_3 , C_4 , C_5 , and C_6 species indicate that many such molecules do give significant mass 28 EI fragment peaks, however, they also tend to give strong peaks at mass 27 and/or mass 29 [28]. We can, therefore, conclude that the principal carrier of the 28 signal is EI of a pyrolysis product with molecular weight of 28, and this has to be C_2H_4 . In order to account quantitatively for the contributions from higher-molecular-weight products to the 26 and 28 signals, it is necessary to fit the spectra, as described below.

The CI spectra have a considerable peak at mass 41 at high temperatures, assigned to protonation of a C_3H_4 (propyne) pyrolysis product. The EI results, at first glance, appear to be inconsistent with this assignment. Note that the C_3 region of the high-temperature JP-10 spectra in Fig. 6 has a larger peak for mass 39 than mass 40. In contrast, the NIST EI spectrum of propyne has a large molecular mass peak (mass 40) and smaller peaks for mass 39 and other fragment ions. This apparent discrepancy is resolved when we consider that this mass range has contributions not only from ionization of C_3 neutrals, but also from EI fragmentation of heavier neutral products. In particular, at the highest temperatures, where CPD is decomposed, benzene is the only major heavy product. In the NIST EI spectra of benzene there is no peak at mass 40, but a substantial peak at mass 39. Therefore, we can explain the mass 39:40 ratio observed for JP-10 at the highest temperatures as follows. The mass 40 peak comes entirely from EI of propyne, while the mass 39 peak has contributions from both propyne and benzene. At somewhat lower temperatures where CPD is a significant product, the NIST EI spectra indicates that EI fragmentation of CPD contributes to both mass 39 and mass 40, consistent with the observation that

the 39:40 ratio changes substantially in this temperature range. These results confirm that C_3H_4 is a major pyrolysis product of JP-10.

From the CI spectra, it was not possible to identify a single C_4H_x product responsible for the set of peaks appearing in the high-temperature JP-10 spectrum (mass 55 with smaller peaks at 57 and 53). In EI of JP-10 at high temperatures, we observe intense peaks at mass 50, 51, and 52, with weaker peaks at mass 53 and 54. The peak at mass 51, along with some intensity at masses 50 and 52, is attributable to EI-induced fragmentation of benzene—CPD does not fragment significantly to $C_4H_x^+$ in EI. After the benzene contributions are subtracted, the balance of the intensity in this mass range (peaks at 50, 52, 53, and 54) must result from EI of some C_4 product or products. The spectra of a number of C_4 species, such as various C_4H_8 isomers, butadiene, 2-butyne, and 1-but-3-yne, are found in the NIST database [28]. All listed C_4H_8 isomers can be eliminated, as they all give substantial peaks at masses 55 and 56, not observed in the JP-10 high-temperature results. Butadiene, 2-butyne, and 1-but-3-yne have peaks at the right masses, but with intensity ratios different from that observed in the high temperature JP-10 results. We conclude that one or more C_4 species are produced in JP-10 pyrolysis, but it is either a mixture, or a C_4 isomer not in the database.

3.4. Data fitting and JP-10 breakdown

To extract quantitative JP-10 breakdown vs temperature results, the set of JP-10 pyrolysis mass spectra were fit, using a contracting-grid least-squares program developed for this purpose. The routine allows penalties to be assigned for nonphysical fits (e.g., for negative residual peaks). The CI and EI spectra were fit independently and the results subsequently merged, as described below. In both cases, the raw experimental spectra were first fit to generate stick spectra. These stick spectra were then fit as linear combinations of basis spectra, where the basis spectra were similarly generated stick spectra for known or suspected product species. Recall that the ion source is held at constant temperature and pressure, independent of flowtube temperature, and that there are sufficient collisions with buffer gas to equilibrate the gas entering the source prior to ionization. As a consequence, the basis spectrum for any given compound should be independent of flowtube temperature, at least up to the point where the compound begins to decompose. The EI spectra were fit over the mass range from 20 to 140; however, with the likely exception of H_2 , which we are unable to monitor for experimental reasons, there are no significant peaks in the experimental spectra below mass 20. The CI spectra were fit

only over the mass range from 40 to 140, as there is too much hydrocarbon background at lower masses. As noted above, no significant signal was observed in either EI or CI in the mass range from 140 to 300.

The basis spectra used in the fits were generated as follows. For EI, where a library of standard spectra is available [28], the basis spectra were simply these standard spectra for the various possible pyrolysis products identified from the combination of EI and CI results, discussed above. EI basis spectra were included for C_2H_2 , C_2H_4 , propyne, CPD, benzene, and JP-10. No standard spectrum is available for JP-10 itself, and we simply used our spectrum taken for the room-temperature flowtube. For CI, no standard spectra are available. For JP-10 and the two major high-molecular-weight pyrolysis products, CPD and BEN, we simply used our experimental CI spectra measured for the room-temperature flowtube. It is clear from both CI and EI data that C_3H_4 (propyne) is a significant pyrolysis product, detected as $C_3H_5^+$ (mass 41) in CI. To represent this product, a basis spectrum consisting of a single peak at mass 41 was used. These four basis spectra (JP-10, BEN, CPD, propyne) account for most of the intensity observed in the CI spectra, and the same species, with the addition of C_2H_2 and C_2H_4 , also account for most of the EI spectral intensity.

In addition, however, both EI and CI results indicate the presence of at least three additional minor products, more clearly seen in CI, where there is less fragmentation. There are clearly one or more C_4H_x products, and as described above, neither the CI nor EI peak patterns allows clear identification. In the case of CI, the basis spectrum for C_4H_x was generated simply by taking the mass 50 to 56 range from the experimental high temperature JP-10 CI spectra, because none of the other major pyrolysis products contribute significantly to this mass range in CI. For EI, we generated a synthetic C_4H_x spectrum from the standard spectra for butadiene, 2-butyne, 2-butene, and 1-but-3-yne, adjusting the contributions of each component to approximately match the experimental high-temperature JP-10 spectrum in the mass 50 to 56 range, after first subtracting the contribution from dissociative ionization of benzene. Note: we do not claim any significance for the particular combination of standard spectra used in this composite—it is simply a convenient way to generate a “ C_4H_x ” spectrum.

Both EI and CI at high temperature also have a pair of weak peaks indicating one or more minor C_7H_x product(s). For CI, we included a basis spectrum consisting of these C_7H_x peaks taken from the high-temperature spectra. For EI these peaks are so weak that they were simply allowed to fall into the category of “unfit residuals.” The CI spectra at high

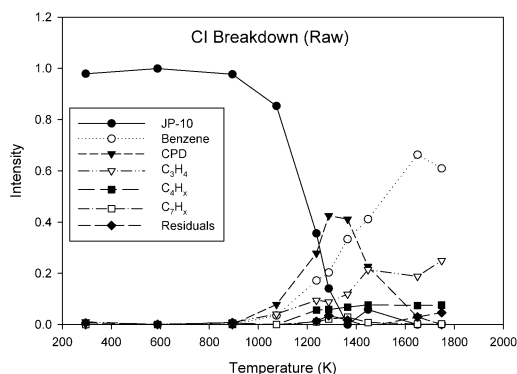


Fig. 7. JP-10 breakdown by CI.

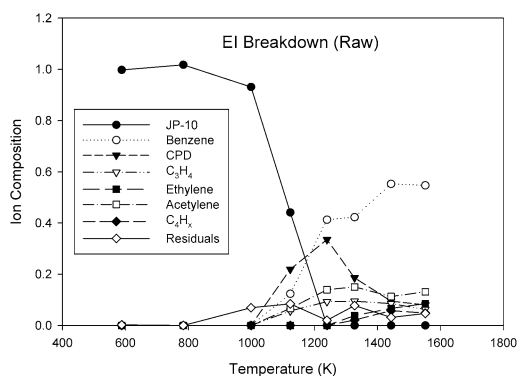


Fig. 8. JP-10 breakdown by EI.

temperatures also have weak groups corresponding to C_8H_x and $C_{10}H_x$. Because these are so weak, they were allowed to fall into the unfit residuals.

The CI fitting results are given in Fig. 7, and the EI fitting results are given in Fig. 8. Note that these figures give the contribution of each basis spectrum to the total ion signal at each temperature. Analysis to extract the desired neutral concentrations is discussed below. Note also that the sum of the contributions at each temperature is normalized to unity in each figure, thus because different numbers of components are included in the CI and EI fits, the normalizations are somewhat different. The two data sets are merged below. In general, the EI and CI data are in good agreement. JP-10 begins to decompose between 900 and 1000 K and is completely decomposed by ~ 1350 K. Initially, CPD is a major product, but it is replaced by other products at higher temperatures. The major high-temperature products are benzene, propyne, C_2H_2 , C_2H_4 , with smaller amounts of C_4H_x and C_7H_x . The data series labeled “Unfit Residuals” in the CI results mostly consists of a variety of minor C_8 and C_{10} species not included in the fits, and the fact that the residuals are so small is a good indication of the fit quality. The “Unfit Residuals” is

larger for EI, for several reasons. The EI residuals at high temperatures partly reflect the fact that the EI fits do not include a basis spectrum for C_7H_x , which was separately broken out in the CI fits. The major reason for the higher EI residuals, especially at low temperatures, is that the EI spectra for individual compounds are not completely independent of flowtube temperature, contrary to what is assumed in the fitting process. This effect can be seen by noting that the JP-10 EI spectrum changes slowly with temperature in the range below 900 K, where JP-10 has not started to decompose. This dependence on flowtube temperature probably results from the lower ion-source pressure under EI conditions, which apparently is insufficient to equilibrate the analyte molecules at the ion-source temperature prior to ionization. Because fitting under these conditions is less reliable, the analysis below will rely mostly on the CI results. The EI results are used only to determine the concentrations of low-molecular-weight products and to confirm the identification of the CPD and benzene products, as discussed above.

Figs. 7 and 8 show compositions as a fraction of the ion signal in the CI and EI mass spectra. To convert these to the fractional composition of the neutral species exiting the flowtube, it is necessary to correct for variations in ionization efficiency for the different compounds. Note that this correction does not affect the temperature dependence derived for any given compound (e.g., JP-10), but only the relative contributions of the different compounds to the product distribution.

For CI, ionization is primarily by proton transfer in the CI source, and the relative efficiency is determined by the product of the collision cross section and the proton-transfer efficiency per collision. Fortunately, the literature is full of examples of proton-transfer rate constants [33], and in every case where the proton transfer reaction is exothermic, the reaction occurs on every collision. In our case, the dominant CI reaction is $CH_5^+ + M \rightarrow MH^+ + CH_4$; thus the reaction exothermicity depends on the difference in proton affinity between M and CH_4 , $\Delta PA(CH_4)$. CH_4 is used in CI precisely because it has an unusually low proton affinity. As a consequence, the proton transfer reactions are highly exothermic for all species of interest, and this correction factor is, therefore, unity for all species.

Under the thermal conditions in the CI source, the collision cross section is accurately given by the capture cross section (σ_{cap}) [34], which can be calculated knowing only the polarizabilities and dipole moments of the analyte molecules. These are known for some analyte molecules, and the rest can be easily calculated using quantum chemistry methods. Quantum chemistry calculations at the B3LYP/6-31G*

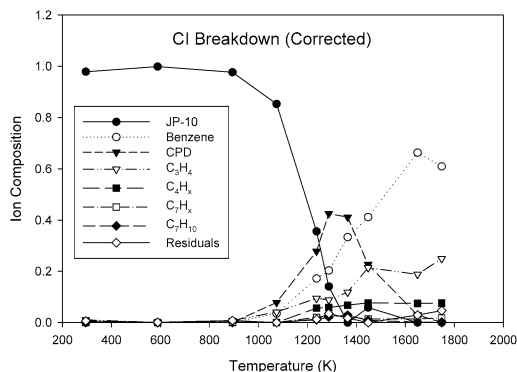


Fig. 9. JP-10 breakdown by CI, corrected for ionization efficiency.

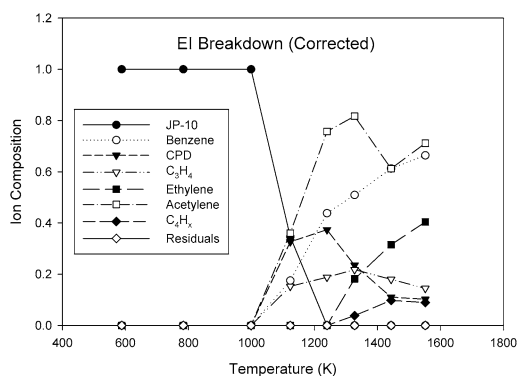


Fig. 10. JP-10 breakdown by EI, corrected for ionization efficiency.

level were performed using GAUSSIAN 98 [29]. In cases where identity of the product species is not clear (C_4H_x , C_7H_x , ...), the values used were averages for several representative molecules. The relative capture cross section for the various products, $\sigma_{cap}(\text{product})/\sigma_{cap}(\text{JP-10})$, ranges from ~ 0.73 (propyne) to ~ 1.1 ($C_{10}H_x$). Fig. 9 presents the CI data after correction, renormalized to that the sum of all contributions at each temperature is unity.

The EI data also need to be corrected for the electron impact ionization efficiency, i.e., for variation in the electron impact ionization cross section from molecule to molecule. The EI cross sections are not known for most of the molecules of interest, but a number of studies have been reported aimed at formulating rules for estimating electron impact ionization cross sections in terms of polarizabilities or other simply determined molecular parameters. For example, Flaim and Ownby [35] and Nishimura and Tawara [36] report linear dependence of the ionization cross section on the number of electrons in the molecule. The linear scaling appears to be reasonably good (within 10%) except for species such He and Ne

with unusually compact electron clouds. Given that all the molecules of interest for our purposes are hydrocarbons, i.e., all the same class of molecule, linear scaling of ionization efficiency with electron count is adequate for correcting our EI data. Fig. 10 gives the corrected EI breakdown data, i.e., fractional neutral composition in the flowtube exhaust. To allow direct comparison with the CI experiments, where acetylene and ethylene were not detected, these two products were excluded from the normalization in Fig. 10.

As noted, we feel that the product distribution inferred from the CI data is more reliable because the higher source pressure appears to thermalize the analyte molecules prior to detection, as is assumed in the fitting process. In addition, CI results in little fragmentation of most of the product species, simplifying the fitting process. We will therefore use the CI product distribution, simply adding the C_2H_2 and C_2H_4 contributions deduced from EI. To give an idea of how well the two data sets agree, it is useful to compare the magnitudes of the CPD and benzene contributions inferred from CI and EI, as shown in Figs. 9 and 10. Note that the onset temperature and qualitative temperature dependence for each product are the same in CI and EI; however, the CPD:benzene ratio differs, as does the temperature where CPD begins to decrease. It is not clear if this discrepancy is a real discrepancy between EI and CI, or simply reflects the greater uncertainty in interpreting the EI data. The differences in EI and CI experimental conditions are the buffer gas (Ar for CI, He for EI), the gas density ($\sim 50\%$ higher for CI than EI), and the residence time ($\sim 30\%$ longer for CI than EI). It is not obvious why any of these differences would result in the differences inferred from fitting the CI and EI spectra, but because the mechanism for CPD and benzene production is not known (see below), a real difference cannot be excluded. It is certainly true that there is higher uncertainty for EI, resulting both from the more extensive fragmentation in EI and the possibility that the product temperature is not fully equilibrated to the ion source under EI conditions. Fig. 11 shows the combined results, normalized such that the sum of all components at each temperature is unity. In this figure we plot the mole fraction of each component at each temperature. Fig. 12 shows the same results, renormalized to show mass fraction.

JP-10 begins to decompose at around 1000 K and is completely decomposed by ~ 1350 K. At low temperature CPD is the main product, but it is unstable at high temperature and begins to decompose at around 1350 K. The major high-temperature products are benzene, propyne, C_4H_x , acetylene, ethylene, and a variety of minor C_8 and C_{10} species, grouped under "Unfit Residuals" in the figure.

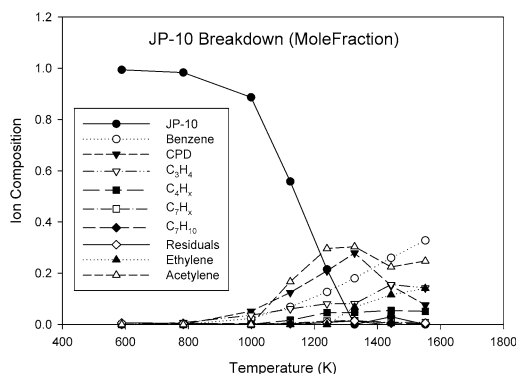


Fig. 11. JP-10 breakdown product distribution, plotted as mole fraction.

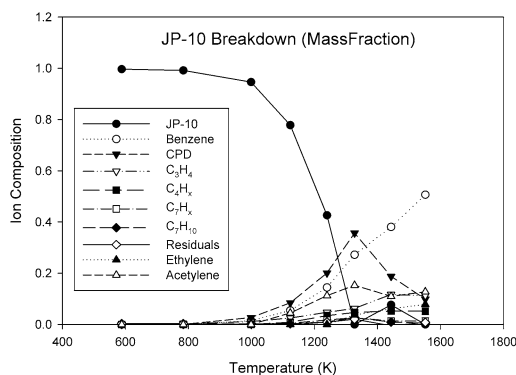


Fig. 12. JP-10 breakdown product distribution, plotted as mass fraction.

3.5. Comparison of experimental and computational results

One of the purposes of these experiments was to test available mechanisms for JP-10 breakdown and combustion proposed by Williams and co-workers [24,37]. This mechanism provides no direct route to either benzene or CPD (although there is a route to cyclopentene), which are major products of the initial decomposition. Violi and Marsh were kind enough to provide us with some preliminary kinetic calculations, based on a mechanism that combines the reduced JP-10 mechanism of Williams et al. [1], augmented by additional reactions from a mechanism developed for a JP-8 surrogate fuel by Violi et al. [38]. The reaction conditions in their simulation (266 Pas neat JP-10, 20–100 ms reaction time) are different from ours (~3% JP-10 in several hundred Pas of rare gas and 2–10 ms reaction time); nevertheless, the comparison clearly shows the need for additional mechanism development. The calculated distribution is dominated by C_2 products even at the onset of JP-10 decomposition, reflecting the fact that the mechanism includes several fast reactions that break JP-10

directly down to C_2 species. The calculations also predict insignificant concentrations of CPD at all temperatures, and the benzene mole fraction is never above ~0.1, compared to 0.33 experimentally. The failure to predict the CPD and benzene concentrations suggests that the mechanism needs to be augmented by additional reactions that generate these species directly from JP-10, rather than only by secondary reactions of primary products. Developing such chemistry is the focus of Violi and Marsh's on-going work.

Acknowledgments

We gratefully acknowledge Niveditha Krishnamoorthy, Nathan Marsh, and Angela Violi for providing the results of their preliminary kinetic modeling for comparison with our data, and for helpful discussions. This work was supported by the Office of Naval Research, Grant N00014-01-1-0541.

References

- [1] S.C. Li, B. Varatharajan, F.A. Williams, *AIAA J.* 39 (2001) 2351–2356.
- [2] N.K. Smith, W.D. Good, *AIAA J.* 17 (1979) 905–907.
- [3] J.E. Peters, A.M. Mellor, *J. Energy* 7 (1982) 95–96.
- [4] R. Atkinson, S.M. Aschmann, W.P.L. Carter, *Int. J. Chem. Kinet.* 15 (1983) 37–50.
- [5] G.W. Burdette, U.S. Patent 4410749, United States Dept. of the Navy, USA, 1983.
- [6] G.A. Szekeley Jr., G.M. Faeth, *Combust. Flame* 49 (1983) 255–259.
- [7] P. Antaki, F.A. Williams, *Combust. Flame* 67 (1987) 1–8.
- [8] L.C. Clausen, T.X. Li, C.K. Law, *J. Propuls. Power* 4 (1988) 217–221.
- [9] F. Takahashi, F.L. Dryer, F.A. Williams, in: *Symp. (Int.) Combust.*, [Proc.] 21st, 1988, pp. 1983–1991.
- [10] S.C. Wong, S.R. Turns, *Combust. Sci. Technol.* 66 (1989) 75–92.
- [11] S.Y. Cho, F. Takahashi, F.L. Dryer, *Combust. Sci. Technol.* 67 (1989) 37–57.
- [12] F. Takahashi, I.J. Heilweil, F.L. Dryer, *Combust. Sci. Technol.* 65 (1989) 151–165.
- [13] S.J. Guisinger, M.E. Rippen, *Prepr. Am. Chem. Soc. Div. Pet. Chem.* 34 (1989) 885–896.
- [14] S.C. Wong, A.C. Lin, *Combust. Flame* 89 (1992) 64–76.
- [15] H.S. Chung, C.S.H. Chen, R.A. Kremer, J.R. Boulton, G.W. Burdette, *Energy Fuels* 13 (1999) 641–649.
- [16] M.S. Fedorova, Y.V. Denisov, V.K. Potapov, *Russ. J. Phys. Chem.* 47 (1973) 1498.
- [17] A.A. Popov, N.N. Blinov, N.S. Vorob'eva, G.E. Zaikov, S.G. Karpova, *Kinet. Katal.* 22 (1981) 139–145.
- [18] R.C. Inman, M.P. Serve, *Org. Mass Spectrom.* 17 (1982) 220–221.
- [19] R. Herzschuh, H. Kuehn, M. Muehlstaedt, *J. Prakt. Chem.* 325 (1983) 256–260.

- [20] M.V. Nesterov, V.A. Ivanov, V.M. Potekhin, A.I. Grigor'ev, *Zh. Prikl. Khim. (Leningrad)* 57 (1984) 1102–1105.
- [21] Y.T. Lin, C. Lin, K. Liou, S.S. Cheng, M.J. Chang, *J. Chin. Chem. Soc. (Taipei)* 33 (1986) 341–345.
- [22] M. Brossi, C. Ganter, *Helv. Chim. Acta* 71 (1988) 848–858.
- [23] W.V. Steele, R.D. Chirico, S.E. Knipmeyer, N.K. Smith, High-Temperature Heat-Capacity Measurements and Critical Property Determinations Using a Differential Scanning Calorimeter: Results of Measurements on Toluene, Tetralin, and JP-10, *Natl. Inst. Pet. Energy Res., Bartlesville, OK, USA*, 1989, p. 42.
- [24] F.A. Williams, R.K. Hanson, C. Segal, in: JANNAF 24th Airbreathing Propulsion Subcommittee and 36th Combustion Subcommittee Joint Meeting, 1999, vol. 1 (692), 1999, pp. 151–161.
- [25] D.F. Davidson, D.C. Horning, J.T. Herbon, R.K. Hanson, *Proc. Combust. Inst.* 28 (2000) 1687–1692.
- [26] Z. Li, J. Eckwert, A. Lapicki, S.L. Anderson, *Int. J. Mass Spectrom. Ion Process.* 167/168 (1997) 269–279.
- [27] Z. Li, S.L. Anderson, *J. Phys. Chem. A* 102 (1998) 9202–9212.
- [28] S.E. Stein, in: W.G. Mallard, P.J. Linstrom (Eds.), NIST Chemistry WebBook, NIST Standard Reference Database Number 69, NIST Mass Spec Data Center, National Institute of Standards and Technology, Gaithersburg, MD, 2000, available at: <http://webbook.nist.gov>.
- [29] M.J. Frisch, G.W. Trucks, H.B. Schlegel, G.E. Scuseria, M.A. Robb, J.R. Cheeseman, V.G. Zakrzewski, J.A. Montgomery, R.E. Stratmann, J.C. Burant, S. Dapprich, J.M. Millam, A.D. Daniels, K.N. Kudin, M.C. Strain, O. Farkas, J. Tomasi, V. Barone, M. Cossi, R. Cammi, B. Mennucci, C. Pomelli, C. Adamo, S. Clifford, J. Ochterski, G.A. Peterson, P.Y. Ayala, Q. Cui, K. Morokuma, D.K. Malick, A.D. Rabuck, K. Raghavachari, J.B. Foresman, J. Cioslowski, J.V. Ortiz, B.B. Stefanov, G. Liu, A. Liashenko, P. Piskorz, I. Komaromi, R. Gomperts, R.L. Martin, D.J. Fox, T. Keith, M.A. Al-Laham, C.Y. Peng, A. Nanayakkara, C. Gonzalez, M. Challacombe, P.M.W. Gill, B.G. Johnson, W. Chen, M.W. Wong, J.L. Andres, M. Head-Gordon, E.S. Replogle, J.A. Pople, GAUSSIAN 98, Gaussian, Pittsburgh, PA, 1998.
- [30] S.G. Lias, J.F. Liebman, R.D. Levin, *J. Phys. Chem. Ref. Data* 13 (1984) 695–808.
- [31] M.S. Fedorova, Y.V. Denisov, V.K. Potapov, *Zh. Fiz. Khim.* 47 (1973) 2667–2670.
- [32] D.F. Davidson, D.C. Horning, M.A. Oehlschlaeger, R.K. Hanson, in: 37th AIAA JPC, Salt Lake City, July 2001.
- [33] Y. Ikezoe, S. Matsuoka, M. Takebe, A. Viggiano, *Gas Phase Ion–Molecule Reaction Rate Constants through 1986*, *Mass Spec. Soc. of Japan*, Tokyo, 1987.
- [34] T. Su, M.T. Bowers, in: M.T. Bowers (Ed.), *Gas Phase Ion Chemistry*, vol. 1, Academic Press, New York, 1979, pp. 83–151.
- [35] T.A. Flaim, P.D. Ownby, *J. Vac. Sci. Technol.* 8 (1971) 661–662.
- [36] H. Nishimura, H. Tawara, *J. Phys. B At. Mol. Opt. Phys.* 27 (1994) 4401.
- [37] *Chemical-Kinetic Mechanisms for Combustion Applications*, 2004, available at: maemail.ucsd.edu/combustion/cermech/.
- [38] A. Violi, S. Yan, E.G. Eddings, A.F. Sarofim, S. Granata, T. Faravelli, E. Ranzi, *Combust. Sci. Technol.* 174 (2002) 399–417.